CORE
Metadata, citation and similar papers at core.ac.uk
Provided by NASA Technical Reports Server

N89-20312

Scientific Support for an Orbiter Middeck Experiment on Solid Surface Combustion

Robert A. Altenkirch (PI), M. Vedha-Nayagam (Postdoctoral Fellow), and Nataraj Srikantaiah (Graduate Student)
Department of Mechanical Engineering
University of Kentucky
Lexington, KY 40506

Abstract

The objective of the current study is to determine the mechanism of gas-phase flame spread over solid fuel surfaces in the absence of any buoyancy or externally imposed gas-phase flow. Such understanding can be used to improve the fire safety aspects of space travel by providing information that will allow judicious selections of spacecraft materials and environments to be made.

The planned experiment consists of measuring the flame spread rate over thermally thin and thermally thick fuels in a closed container in the low-gravity environment of the Space Shuttle. The Shuttle provides sufficient time for the spread process to be studied and to evolve to a steady state. Steady spread can be achieved only if the experimental time is long compared to the ratio of the gas-phase kinematic viscosity to the product of the spread rate and a velocity characteristic of the gas. Measurements consist of flame spread rate and shape obtained from two views of the process as recorded on movie film and surface and gas-phase temperatures obtained from fine-wire thermocouples. The temperature measurements along with appropriate modelling provide information about the gas-to-solid heat flux. Environmental parameters to be varied are the oxygen concentration and pressure.

In support of the proposed space-based experiments, ground-based experiments have been used to prove the sample ignition system and provide limited information about flame shapes and spread rates in the experimental time available in the droptower facilities at Lewis Research Center. Additionally, a theoretical modelling effort is being conducted to aid in elucidating the physics of the flame spread process.

Numerical computations of the theoretical problem appear to show that it is necessary to account for the fact that, with respect to the quiescent oxidizer, the flame is moving. In flame-fixed coordinates then, the flame sees a gentle forced flow of speed equal to the spread rate. Attempts to neglect this flow as being unimportant with respect to the flow established by the interfacial velocity appear to indicate that a consistent, steady-state coupling between the gas and solid phases is not possible under this circumstance. The relative flow is responsible for removing convectively the energy released by chemical reaction in the gas to allow the steady-state to be maintained.

PRECEDING PAGE BLANK NOT FILMED

Introduction

A gas-phase flame spreads over the surface of a solid, pyrolyzing combustible by tranferring heat, either through the gas or the solid, ahead of itself to raise the temperature of the virgin fuel to a pyrolysis temperature [1]. The characteristics of the spreading flame and the forward heat transfer depend on the gas-phase flow field in which the flame is embedded. In most flame spread studies, the flow field is established by natural (see, e.g., [2-4]) or externally imposed forced (see, e.g., [5,6]) convection superimposed on the flow resulting from the phase change at the fuel-gas interface. Little is known about the physics of the process as it would occur in a flow field established by the phase change alone.

The flow induced by flames spreading in the Earth's gravitational environment may be either in the same or opposite direction to that of spread depending on the direction of spread with respect to the Earth's gravity. In upward propagating flames, that is those oriented so that a component of gravity is in the direction of spread, the spread process is rapid and acceleratory [7]. The induced flow is in the direction of spread, and the hot combustion products form a plume that bathes the unburnt fuel, heating it by conduction and, if the optical depth of the flame is large enough, by radiation as well. In downward flame spread, buoyancy induces a flow of ambient fluid that opposes the spreading flame as shown in Fig. 1 where U_∞ is the speed of the induced flow. The result is that the forward heat transfer occurs either by heat conduction through the gas or solid (or both) [3,4]. Radiation heat transfer is usually unimportant because the

flame, due to the buoyant flow, lies close to the fuel surface resulting in a small view factor. And, the convective motion cools the unburnt fuel rather than heating it.

Horizontally spreading flames possess some of the same characteristics as both downward and upward spreading flames do. Topside flames must spread into an opposing flow of oxidizer that is induced by the flame plume as in downward spread, but unlike downward spread, the flame plume extends above the pyrolyzing surface of the fuel to provide a favorable view factor for forward radiation heat transfer [8,9]. Underside flames induce a flow in the direction of spread. They tend to propagate unsteadily and race ahead of the topside flame [10,11].

Photographs of flames spreading over thin cellulose acetate sheets at nearly zero gravity show that these low-gravity flames are similar in appearance to downward spreading flames at normal gravity [12,13]. They do not exhibit a plume that precedes the leading edge of the flame as in upward spread, and the flames on both sides of the fuel bed look the same, as they do in downward spread, in contrast to horizontal spread. It is likely then that the physics of flame spreading in low gravity is more akin to that of downward spread in normal gravity rather than either upward or horizontal spread. Further support of this speculation is given by the fact that low-gravity spread rates are just less than downward spread rates at normal gravity, which in turn are lower than either horizontal or upward spread rates, upward ones being the highest [7,12].

Downward Flame Spread

Gas-phase conduction is the dominant mode of forward heat transfer in downward flame spread (and for spreading into a forced flow) for fuels that are heated across their entire thickness (thermally thin) downstream of the leading edge of the flame and also have a large ratio of the gas-phase conduction length (gas thermal diffusivity divided by opposing flow velocity) to the solid-phase forward conduction length (solid thermal diffusivity divided by flame spread rate). In this case, an increase in the strength of the buoyant flow can only cause the spread rate to fall. The reason for this is that the residence time of the fuel vapors near the leading edge of the flame is reduced relative to the time that the exothermic reactions require for completion so that the flame temperature drops, reducing the forward heat tranfer and hence the spread rate. This phenomenon can be expressed in terms of the Damkohler number, a ratio of the residence time to the reaction time. For large Damkohler number, the spread rate is unaffected by changes in the Damkohler number because sufficient reaction time is provided for the production of the highest temperature attainable. For small Damkohler number, the spread rate decreases as the Damkohler number decreases [3].

The dominant heat transfer mode depends on the Damkohler number for fuels that are thick enough so that they may or may not be heated across their entire thickness [4]. At large Damkohler number, the heated layer thickness in the fuel is small compared to the fuel's thickness (thermally thick), and the ratio of the gas-phase to solid-phase conduction length exceeds unity; heat transfer occurs then by gas-phase conduction.

Increasing the strength of the opposing flow does not change the flame temperature or the heat conducted upstream in the gas because the conduction length scale in the gas is the same parallel and normal to the fuel surface, but it decreases the heated layer depth in the solid. The reduced in-depth heating results in more of the forward heat transfer being available for vaporization with a concomitant increase in spread rate [4]. At small Damkohler number, as the flame nears extinction, nearly the entire fuel thickness is heated, and forward heat transfer is by solid-phase conduction [1,14]. Increasing the buoyant flow here decreases the flame temperature causing a reduction in the forward heat transfer and hence a reduction in the spread rate.

As is evident from the above discussion, the direction and strength of the gas-phase flow are of signal importance in establishing the spread rate. For downward spread, the character of the flow field and the physics of the process are reasonably well understood. The degree of this understanding is demonstrated by the success with which dimensionless downward flame spread rates, $\bar{V}_F$ where

$$\bar{V}_F = \frac{\rho_s C_s V_F \tau}{2^{1/2} k} \left(\frac{T_v - T_\infty}{T_f - T_v} \right) \tag{1}$$

are correlated against a Damkohler number [3-5], $\bar{B}$, where

$$\bar{B} = \frac{B k m_{ox,\infty}}{M_{ox} C_p v_c^2} \left(\frac{\bar{T}_f^2}{\bar{T}_a} \right)^3 e^{-(\bar{T}_a/\bar{T}_f)} \tag{2}$$

The dimensionless spread rate $\bar{V}_F$ is a ratio of the actual heat transferred

forward of the flame to the maximum that could be transferred if $\tilde{B}$ were large and the flame were at its maximum temperature [3]. In the above, ρ_s is the solid-phase density, C_s is the solid-phase specific heat, V_F is the spread rate, k is the gas-phase thermal conductivity, T_v is the vaporization temperature, T_∞ is the ambient temperature, T_f is the flame temperature for adiabatic stoichiometric combustion, τ is the heated layer depth in the solid, B is the preexponential factor for an assumed second-order reaction, $m_{ox,\infty}$ is the ambient oxygen mass fraction, M_{ox} is the molecular weight of oxygen, C_p is the gas-phase specific heat at constant pressure, v_c is the characteristic, gas-phase velocity, which in Fig. 1 would be U_∞, and $\tilde{T}_f$ and $\tilde{T}_a$ are the flame and activation temperature, respectively, measured in the units of $\Delta H_c m_{ox,\infty}/iC_p$ where ΔH_c is the heat of combustion of gas-phase fuel, and i is the mass of oxygen needed to oxidize a unit mass of fuel. For thermally thin fuels, τ is the fuel bed half-thickness while for thick fuels, τ depends on v_c but is independent of the fuel bed thickness [4].

The expression for $\tilde{V}_F$ above derives from a solution to the constitutive equations that govern flame spread into an opposing flow of oxidizer of uniform speed v_c when $\tilde{B}\to\infty$ [6] such that $\tilde{V}_F$ is unity. The parameter $\tilde{B}$, with which $\tilde{V}_F$ correlates for finite $\tilde{B}$, obtains, in part, from dimensional analysis [3]. Examples of the manner in which $\tilde{V}_F$ correlates with $\tilde{B}$ are shown in Figs. 2 and 3 for downward spread over thin paper samples and thick samples of polymethlymethacryalate (PMMA) where τ has been set equal to $[2^{1/2}k_s\ (T_v - T_\infty)]/[\rho C_p v_c (T_f - T_v)]\ (1 + 0.5\ \tan\phi)$ with k_s the solid-phase thermal conductivity, and ρ the gas-phase density [6]. The item in parentheses that contains ϕ, where ϕ is the regression angle in the pyrolyzing region measured with respect to the plane in which the unburnt

fuel surface lies, accounts for surface regression [14]. The characteristic, gas-phase velocity for downward spread that was used in Figs. 2 and 3 is v_b, the buoyant velocity $(\nu g \Delta H_c m_{ox,\infty}/T_\infty i C_p)^{1/3}$ where ν is the kinematic viscosity, and g is the acceleration of gravity. This form for v_c reflects the fact that the important induced flow velocity is that near the leading edge of the flame, where boundary layer assumptions are invalid. As a result, the Peclet number there must be of order unity such that there is no independently specifiable length [15]. Dimensional analysis then leads to the expression given for v_b [3].

Changes in $\bar{B}$ in Figs. 2 and 3 were brought about by changes in $m_{ox,\infty}$, the environmental pressure, P, and the acceleration of gravity, the major controllable dimensional parameters that affect the buoyant flow. Parameter variation was accomplished by performing the spread rate experiments in a closed chamber that was swung on a centrifuge so that gravitational accelerations above those of the Earth's normal acceleration, g_E, were obtained. Increases in v_b, e.g., through increases in g, cause $\bar{B}$ to decrease, which results in a decrease in flame temperature for small $\bar{B}$. As $\bar{B}$ decreases, $\bar{V}_F$ decreases for small $\bar{B}$ indicating a reduction in the forward heat transfer compared to the maximum that could be transferred if $\bar{B}$ were large.

Flame Spreading at Reduced Gravity

Results in Figs. 2 and 3 can be used to estimate spread rates at reduced gravity. In Fig. 4 we compare spread rates for flame spread down thick PMMA fuel beds determined from the correlation of Fig. 3 and computed

from the theoretical treatment of Refs. [16] and [17]. The discrepancy between measured spread rates and those determined from the correlation, which derives from experiment, is because of a slightly different definition of the vaporization temperature in Figs. 3 and 4 [17].

In the theory, it is assumed that the gas-phase chemistry is infinitely fast and that an appropriately defined Grashof number is large. The gas-phase flow, temperature, and species fields were determined through the application of matched asymptotic expansion for large Grashof number [17]. The flow then is taken to be established by buoyancy, and for the conditions shown, $\tilde{B}$ is large enough for g less than about 10^{-1} g_E to make the assumption of infinite-rate chemistry valid. Beyond 10^{-1} g_E, the discrepancy between theory and correlation is due to finite-rate chemistry effects, and below 10^{-3} g_E the theory fails because the Grashof number is not large. The flow then for $g < 10^{-3}$ g_E is not dominated by buoyancy, and the normal flow at the surface with velocity v_s due to pyrolysis becomes important. In this circumstance, the correlations of Figs. 2 and 3 are no longer valid because of the use of v_b for v_c.

With the characteristic length in the Grashof number set equal to ν/v_s, whether or not buoyancy induced flows are important depends on the magnitude of $(v_b/v_s)^3$ [18]. Realizing that the fuel pyrolyzes according to an Arrhenius decomposition law, we get approximately that

$$(v_b/v_s)^3 \propto g m_{ox,\infty} P^2 \exp(E_s/RT_s) \qquad (3)$$

where in the above proportionally E_s is the activation energy for pyrolysis, R is the gas constant, T_s is the surface temperature, and the temperature dependence of gas-phase properties such as viscosity, density, specific

heat, etc. have been neglected because their effect is overwhelmed by the temperature dependence of the Arrhenius term. The controllable parameters in Eqn. (3) are g, $m_{ox,\infty}$, and P, and T_s is determined by these controllable parameters. Buoyancy can be rendered unimportant then if $(v_b/v_s)^3$ can be made small compared to unity by conducting experiments at reduced $m_{ox,\infty}$, P, and/or g.

Reducing $m_{ox,\infty}$ to minimize buoyancy is impractical because approximately less than an order of magnitude reduction can be achieved from pure oxygen before extinction is encountered. Additionally, a reduction of $m_{ox,\infty}$ results in a reduction of T_s because of the reduced flame temperature and resultant heat flux back to the fuel bed. The reduction in T_s causes the exponential term in $(v_b/v_s)^3$ to increase such that, practically, it is unclear whether or not a decrease in the velocity ratio is achieved by a decrease in $m_{ox,\infty}$.

Reducing pressure to achieve a small value of the velocity ratio is more attractive than reducing $m_{ox,\infty}$ because the ratio is more sensitive to pressure. A three order of magnitude change in $(v_b/v_s)^3$ can be achieved by changes in pressure, but at low pressures, extinction is encountered at the lower oxygen concentrations.

Reductions in gravitational acceleration can be used to acheive the desired goal, and it would appear that the largest reductions in $(v_b/v_s)^3$ can be had, about five to six orders of magnitude, through reductions in g. Uncertainties in the kinetic constants of pyrolysis make it difficult to determine quantitatively accurate values of the gravitational acceleration necessary to achieve small values of $(v_b/v_s)^3$, but for the conditions of

Fig. 4, levels below 10^{-3} g_E are needed.

Based on a detailed assessment of the gas-phase physics of flame spreading as described above, a Space Shuttle-based experimental program has been developed [19]. Although ground-based techniques for conducting reduced-gravity experiments can be used to obtain some useful information, the time available in a droptower is, in general, not sufficient to study the process adequately or develop a steady state. Aircraft flying parabolic trajectories do not appear to provide a sufficiently low gravitational acceleration to yield quantitative results, and the acceleration present can exist in more than one direction. Below we briefly describe the experiment and the modelling effort that is being conducted to support it. Detailed requirements of the experimental design can be found in Refs. [18] and [19].

Experiment

The experiment consists of measuring the flame spread rate, the surface temperature, and the gas-phase temperature, at two locations at different distances from the fuel bed surface, for rectangular samples of ashless filter paper, a thermally thin fuel, and PMMA, a thermally thick fuel. These fuels were chosen because of the flame spread data that are available on them. Additionally, ashless filter paper is about the thinnest sample for which the solid temperature can be measured using fine-wire thermocouples, which is the technique used for measuring temperatures.

Spread rates are obtained from color movies of the spread process. Two cameras are used to obtain an edge view of the flame and a view of the fuel surface over which the flame is spreading. The sample is held in the center

of an environmental chamber as shown schematically in Fig. 5. It is ignited at one end using a heated nichrome wire coated with nitrocellulose.

Chamber volume, which is about 0.039 m^3, was chosen such that the oxygen present in the chamber would not be depleted more than 5% as a result of the combustion of the fuel. Sample size, which is 10 cm by 3 cm for the filter paper and 0.318 cm thick by 2 cm long by 0.635 cm wide for the PMMA, was chosen in conjunction with the chamber sizing and is typical of sample sizes that have been used in ground-based experiments [3,4]. The paper sample is clamped between thin metal plates while the sides and bottom of the PMMA sample are to be insulated.

In addition to oxygen depletion considerations, heat loss from the sides of the paper sample was taken into account in choosing the size of the sample. Ideally, the sides should be insulated so as not to complicate the process with heat loss to the sample holder. Insulating the sides of the paper sample is impractical, so it is made wide enough so that the heat lost to the sample holder is unimportant. The data in Fig. 2 for $m_{ox,\infty} = 0.329$ and $m_{ox,\infty} = 0.774$ that seem not to follow the general correlation between $\bar{V}_F$ and $\bar{B}$ were obtained under conditions where heat loss to the sample holder was not insignificant. The result is that another dimensionless parameter is introduced such that $\bar{V}_F$ is no longer a function of $\bar{B}$ alone [3].

The experimental apparatus for the paper samples has been tested in the NASA-Lewis Research Center 5 s droptower facility. Tests were completed to prove the ignition system and choose an experimental matrix. The proposed test matrix consists of environments composed of 30% to 50% O_2 in N_2 and pressures from 1.0 to 2.0 atm.

Some preliminary results for the ashless filter from the droptower

experiments are shown in Figs. 6 and 7. In Fig. 6, an edge photo of three flames spreading from left to right is shown. The scale is that 1 cm on the figure is 0.625 cm of actual length. The light region in the photos is due to luminous radiation. There is a faint, blue flame at the leading edge that is visible in the color photos but does not show in the black-and-white copy.

In Fig. 6, the progression of the pyrolysis front as a function of time for what is labelled Case 1 in Fig. 6 is shown. From the figure, the spread rate, which can be calculated to be about 0.32 cm/s for comparison to the measured downward spread rate of 0.86 cm/s, appears rather steady.

Some unsteadiness in the overall process was present though in that the distance between the pyrolysis front and the luminous portion of the flame was increasing, indicating that the blue flame region at the leading edge of the flame was growing.

Modelling

In support of the experimental effort, a modelling effort is being conducted to provide insight for interpretation of the experimental results. The mathematical problem in dimensionless form for steady flame spreading in the absence of buoyancy over a thermally thin fuel in which solid-phase conduction is neglected is given below. A schematic of the region to which the equations apply is shown in Fig. 8.

Line S is an approximate line of symmetry through the pyrolysis region that we use in one version of the problem that we have investigated. Assumptions inherent in the formulation, which is for properties evaluated

at a reference temperature intermediate between the ambient temperature and the flame temperature, are the usual ones (see, e.g., Ref. [20]) and will not be discussed here.

Continuity

$$\frac{\partial \rho u}{\partial x} + \frac{\partial \rho v}{\partial y} = 0 \tag{4}$$

Momentum

$$\rho u \frac{\partial u}{\partial x} + \rho v \frac{\partial u}{\partial y} = - \frac{\partial P}{\partial x} + \frac{\mu}{Re} \left(\frac{\partial^2 u}{\partial x^2} + \frac{\partial^2 u}{\partial y^2} \right) \tag{5}$$

$$\rho u \frac{\partial v}{\partial x} + \rho v \frac{\partial v}{\partial y} = - \frac{\partial P}{\partial y} + \frac{\mu}{Re} \left(\frac{\partial^2 v}{\partial x^2} + \frac{\partial^2 v}{\partial y^2} \right) \tag{6}$$

Energy

$$\rho u \frac{\partial T}{\partial x} + \rho v \frac{\partial T}{\partial y} = \frac{k}{Re\ Pr} \left(\frac{\partial^2 T}{\partial x^2} + \frac{\partial^2 T}{\partial y^2} \right) + Q \dot{W}_f''' \tag{7}$$

Species (fuel and oxygen)

$$\rho u \frac{\partial m_f}{\partial x} + \rho v \frac{\partial m_f}{\partial y} = \frac{\rho D}{Re\ Pr\ Le} \left(\frac{\partial^2 m_f}{\partial x^2} + \frac{\partial^2 m_f}{\partial y^2} \right) + \dot{W}_f''' \tag{8}$$

$$\rho u \frac{\partial m_{ox}}{\partial x} + \rho v \frac{\partial m_{ox}}{\partial y} = \frac{\rho D}{Re\ Pr\ Le} \left(\frac{\partial^2 m_{ox}}{\partial x^2} + \frac{\partial^2 m_{ox}}{\partial y^2} \right) + i\dot{W}_f''' \tag{9}$$

In the above, the density, ρ, viscosity, μ, temperature, T, and mass

diffusivity, D, are measured in the units of their ambient values, i.e., at ∞. The pressure, P, is measured in the units of $\rho_\infty v_c^2$. The Reynolds number, Re, Prandtl number, Pr, and Lewis number, Le are

$$Re = \frac{v_c L}{\nu_\infty}; \quad Pr = \frac{\nu_\infty}{\alpha_\infty}; \quad Le = \frac{\alpha_\infty}{D_\infty} \tag{10}$$

with α the thermal diffusivity, and L an arbitrary length. Distances x and y are measured in the units of L. The dimensionless reaction rate is

$$\dot{W}_f''' = - \tilde{B}\rho^2 m_{ox} m_f e^{-T_a/T} \tag{11}$$

with $\tilde{B}$ a Damkohler number defined as

$$\tilde{B} = \frac{BL\rho_\infty}{M_{ox} v_c} \tag{12}$$

M_{ox} is the molecular weight of oxygen, and Q is the heat of combustion divided by $C_p T_\infty$. The equation of state is that $\rho T=1$.

The boundary conditions are:

Right side (R)

$$u = \frac{-V_F}{v_c}; \quad v = m_f = 0; \; m_{ox} = m_{ox,\infty}; \; T = 1 \tag{13}$$

Left side (L)

$$\frac{\partial u}{\partial x} = \frac{\partial v}{\partial x} = \frac{\partial m_f}{\partial x} = \frac{\partial m_{ox}}{\partial x} = \frac{\partial T}{\partial x} = 0 \; ; \; P = \text{constant} \tag{14}$$

Top (T)

$$u = \frac{-V_F}{v_c} \; ; \; \frac{\partial v}{\partial y} = m_f = 0 \; ; \; m_{ox} = m_{ox,\infty} \; ; \; T = 1 \; ; \; P = \text{constant} \tag{15}$$

Upstream fuel surface (U)

$$u = \frac{-V_F}{v_c} \; ; \; v = \frac{\partial m_f}{\partial y} = \frac{\partial m_{ox}}{\partial y} = 0 \; ; \; T = T_s \tag{16}$$

Pyrolysis region (P)

$$u = \frac{-V_F}{v_c} \; ; \; v = \frac{v_s}{v_c} \; ; \; T = T_s \tag{17}$$

$$\dot{m}'' \, (1 - m_{f,s}) = \frac{\rho D}{Re \; Pr \; Le} \frac{\partial m_f}{\partial y} \bigg|_s \tag{18}$$

$$\dot{m}'' \, m_{ox,s} = - \frac{\rho D}{Re \; Pr \; Le} \frac{\partial m_{ox}}{\partial y} \bigg|_s \tag{19}$$

Downstream of burnout (D)

$$\frac{\partial u}{\partial y} = v = \frac{\partial m_f}{\partial y} = \frac{\partial m_{ox}}{\partial y} = \frac{\partial T}{\partial y} = 0 \tag{20}$$

The dimensionless pyrolysis flux, $\dot{m}''$, is taken to be

$$\dot{m}'' = \frac{\rho_s \tau B_s e^{-E_s/RT_s}}{\rho_\infty v_c} \tag{21}$$

where B_s is the preexponential factor for the Arrhenius decomposition.

For the solid phase, the energy and mass conservation equations with x, y, T_s, $\dot{m}''$, and k defined as above are

$$\rho_s \left(\frac{V_F}{v_c}\right) \frac{\partial T_s}{\partial x} = \dot{m}'' \left(\frac{\rho_\infty}{\rho_{s,\infty}}\right) \left(\frac{L}{\tau}\right) (\Delta H_v + (1-C_p)(T_s-1)) + \left(\frac{k_\infty}{\tau C_s v_c \rho_{s,\infty}}\right) k \left.\frac{\partial T}{\partial y}\right|_s \tag{22}$$

$$\left(\frac{V_F}{v_c}\right) \frac{\partial \rho_s}{\partial x} = - \dot{m}'' \left(\frac{\rho_\infty}{\rho_{s,\infty}}\right) \left(\frac{L}{\tau}\right) \tag{23}$$

where ρ_s is measured in the units of the original solid density, $\rho_{s,\infty}$, C_p is measured in the units of C_s, and ΔH_v is the heat of vaporization divided by $C_s T_\infty$. The fuel enters at the right where $\rho_s = T_s = 1$.

If the gas-phase chemistry is infinitely fast, it is convenient to combine the energy and species equations by defining the coupling functions [21]

$$b_{fo} = m_f - \frac{(m_{ox} - m_{ox,\infty})}{i} \; ; \; b_{to} = \frac{T}{Q} + \frac{(m_{ox} - m_{ox,\infty})}{i} \tag{24}$$

The b_i then satisfy, with unity Lewis number,

$$\rho u \frac{\partial b_i}{\partial x} + \rho v \frac{\partial b_i}{\partial y} = \frac{k}{RePr} \left(\frac{\partial^2 b_i}{\partial x^2} + \frac{\partial^2 b_i}{\partial y^2} \right) \qquad (25)$$

The boundary conditions on b_i derive from the above, but they are modified to account for the fact that, for infinite-rate chemistry, inside the flame there is no oxygen, and outside the flame there is no fuel. The flame is located where $m_f = m_{ox} = 0$.

There are not a large number of solutions of similar problems in the literature because of the complexity of the problem and the difficulties in determining the eigenvalue spread rate, but some noteworthy examples are given in Refs. [6,17] and [22] through [25]. We have solved several versions of the above problem using the numerical scheme SIMPLER [26]. The cases that we have considered to date are i) infinite-rate chemistry in the "half-region" in which symmetry conditions are written along S, ii) infinite-rate chemistry in the entire domain, and iii) finite-rate chemistry in the "half-region" and entire domain.

In Problem i), the flame is taken to be symmetrical about the line S, and a unique surface temperature in the pyrolysis region is specified. This decouples the gas and solid phases such that the gas-phase problem is computed as though the flame were stationary, i.e., $V_F \ll v_s$, and as a function of surface temperature. The length L that appears in the problem is set equal to one-half the length of the pyrolysis region, which is estimated from the experiment. Additionally, v_c is set equal to v_s, and along R $\partial(u,v)/\partial x = 0$, and b_i are their ambient values. Along T, y-direction derivatives are zero. We have used this problem to investigate

the characteristics of the fluid mechanics and compute flame shapes for comparison to the droptower experiments, even though the experiments may not have reached steady state.

Coupling function contours for the half-region for Case 1 of Fig. 6 are shown in Fig. 9. The heavy contour is the flame. The scale in Figs. 6 and 9 are the same so that a direct comparison can be made. A surface temperature of 650 K, which is comparable to measured temperatures under similar conditions [27], gives a flame shape that matches the experimental shape adequately.

Using the entire domain and infinite-rate chemistry, (Problem ii) attempts to predict the spread rate with L identified as the length of the pyrolysis region, $v_c = v_s$, and conditions along R, L, and T as in the symmetrical problem failed. If the requirement is made that the the fuel density at burnout drop to some small percentage of its original value, no pyrolysis temperature can be found that is consistent with the gas and solid-phase conservation equations. The reason for this is that the flow in the gas, which is generated solely by the flow in the pyrolysis region, is insufficient to remove the chemical energy that is released in the gas to maintain a steady state. Because the fuel, which is moving at speed V_F in flame-fixed coordinates, contains little mass after the burnout location, it cannot remove the energy either. The result is that no consistent steady-state can be found.

It would appear necessary to include the forced flow of speed V_F that the flame sees in flame fixed coordinates, even though V_F may be small compared to v_s, to remove the chemical energy released. Solving Problem ii)

with v_c defined as an arbitrary reference velocity, v_r, such that u along R is equal to $-V_F/v_r$ and L set equal to α/v_r, steady spread rates can be found. The process is an iterative one of guessing the solution and iterating back and forth betwen the phases until the surface temperature and spread rate do not change substantially from one iteration to another. The resulting spread rate will be valid as long as V_F is approximately equal to v_r. Coupling function contours and a velocity vector field for Case 1 of Fig. 5 are shown in Figs. 10 and 11. The computed spread rate is 2.35 cm/s, as compared to the value gotten from Fig. 7 of 0.32 cm/s. The computed spread rate is larger than what we expect ultimately to measure because of the use of infinite-rate chemistry. We are in the process now of making computations that include the effects of finite-rate chemistry with all other aspects of the procedure the same, i.e., Problem iii).

Summary

Based on a review of the flame spread literature, an experiment to investigate flame spreading in reduced gravity has been designed. Construction of the experiment is, for all practical purposes, complete. The modelling effort that is being conducted in support of the experiment is continuing. To date it has demonstrated the importance of the convective motion that results from the fact that the flame is moving into the oxidizing environment.

References

1. Williams, F.A. (1977). Mechanisms of fire spread, Sixteenth Symposium (International) on Combustion, The Combustion Institute, pp. 1281-1294.

2. Fernandez-Pello, A.C. and Santoro, R.J. (1979). On the dominant mode of heat transfer in downward flame spread, Seventeenth Symposium (International) on Combustion, The Combustion Institute, Pittsburgh, pp. 1201-1209.

3. Altenkirch, R.A., Eichhorn, R., and Shang, P.C. (1980). Buoyancy effects on flames spreading down thermally thin fuels, Combustion and Flame, 37, pp. 71-83.

4. Altenkirch, R.A., Eichhorn, R., and Rizvi, A.R. (1983). Correlating downward flame spread rates for thick fuel beds, Combustion Science and Technology, 32, pp. 49-66.

5. Fernandez-Pello, A.C., Ray, S.R., and Glassman, I. (1981). Flame spread in an opposed forced flow: the effect of ambient oxygen concentration, Eighteenth Symposium (International) on Combustion, The Combustion Institute, pp. 579-589.

6. de Ris, J.N. (1969). Spread of a laminar diffusion flame, Twelfth Symposium (International) on Combustion, The Combustion Institute, Pittsburgh, pp. 241-252.

7. Fernandez-Pello, A.C. (1978). A theoretical model for the upward laminar spread of flames over vertical fuel surfaces, Combustion and Flame, 31, pp. 135-148.

8. Ray, S.R., Fernandez-Pello, A.C., and Glassman, I. (1980). A study of the heat transfer mechanisms in horizontal flame propagation, Journal of Heat Transfer, 107, pp. 357-363.

9. Altenkirch, R.A., Short, J.L., Vedha-Nayagam, M., and Padgaonkar, A.M. (1985). Including radiation heat transfer effects in dimensionless flame spread correlations, Central States-Western States Section/The Combustion Institute.

10. Kashiwagi, T. and Newman, D.L. (1976). Flame spread over an inclined thin fuel surface, Combustion and Flame, 26, 163-177.

11. Hirano, T., Noreikis, S.E., and Waterman, T.E. (1973). Measured velocity and temperature profiles of flames spreading over a thin combustible solid, IIT Research Institute, Interim Technical Report No. 2, Project J-1139.

12. Andracchio, C.R. and Cochran, T.H. (1976). Gravity effects on flame spreading over solid surfaces, NASA TN D-8828.

13. Andracchio, C.R. and Cochran, T.H. (1974). Burning of solids in oxygen-rich environments in normal and reduced gravity, NASA TM X-3055.

14. Altenkirch, R.A., Rezayat, M., Eichhorn, R., and Rizzo, F.J. (1982). Boundary integral equation method calculations of surface regression effects in flame spreading, Journal of Heat Transfer, 104, pp. 734-740.

15. Hellums, J.D. and Churchill, S.W. (1961). Dimensional analysis and natural circulation, Chemical Engineering Progress Symposium Series, 57, pp. 75-80.

16. Vedha-Nayagam, M. and Altenkirch, R.A. (1985). Backward boundary layers in downward flame spread, Twentieth Symposium (International on Combustion, The Combustion Institute, Pittsburgh, pp. 1583-1590.

17. Altenkirch, R.A. and Vedha-Nayagam, M. (1985). Gravitational effects on flames spreading over thick solid surfaces, Acta Astronautica, 12, pp. 565-572.

18. Altenkirch, R.A. and Vedha-Nayagam, M. (1985). Gravitational effects in flame spreading, NASA report on Grants NAG 3-258 and NAG 3-114.

19. Altenkirch, R.A. (1985). Science requirements document for a solid surface combustion experiment, NASA-Lewis Research Center.

20. T'ien, J.S. (1986). The flame front problem: combustion in low-Reynolds-number flow, ASME Paper 86-WA/HT-49.

21. Williams, F.A. (1985). Combustion Theory, Benjamin/Cummings.

22. Frey, A.E., Jr. and T'ien, J.S. (1979). A theory of flame spread over a solid fuel including finite-rate chemical kinetics, Combustion and flame, 36, pp. 263-289.

23. Fernandez-Pello, A.C. and Williams, F.A. (1977). A theory of laminar flame spread over flat surfaces of solid combustibles, Combustion and Flame, 28, pp. 251-277.

24. Sirignano, W.A. (1974). Theory of flame spread above solids, Acta Astronautica, 1, pp. 1285-1299.

25. Chen, C. (1986). Flame propagation: effect of solid-phase heat conduction, Eastern Section/The Combustion Institute.

26. Patankar, S.V. (1980). Numerical Heat Transfer and Fluid Flow, McGraw-Hill.

27. Parker, W.J. (1972). Flame spread model for cellulosic materials, Journal of Fire and Flammability, 3, pp. 254-269.

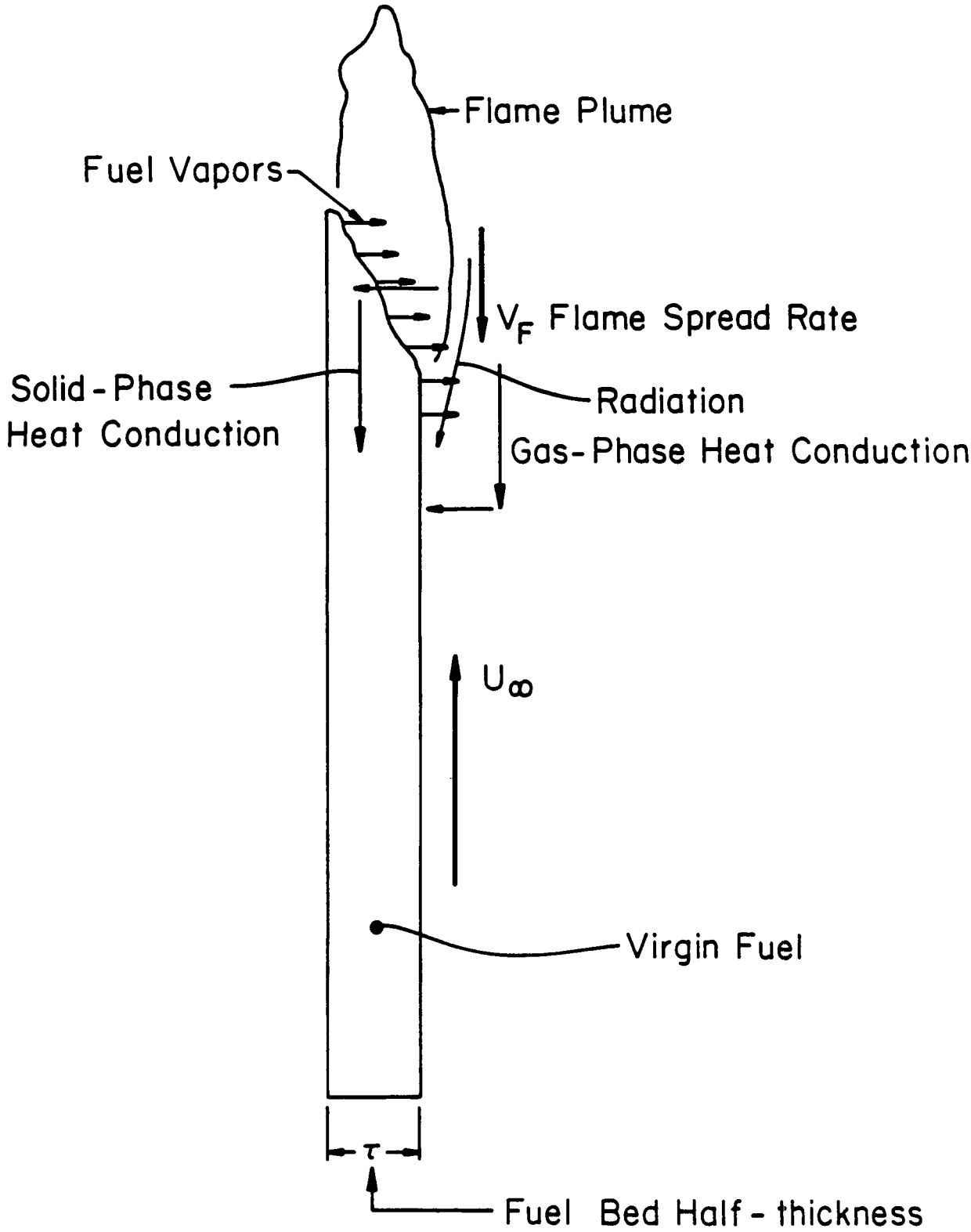

Figure 1 Downward flame spread process.

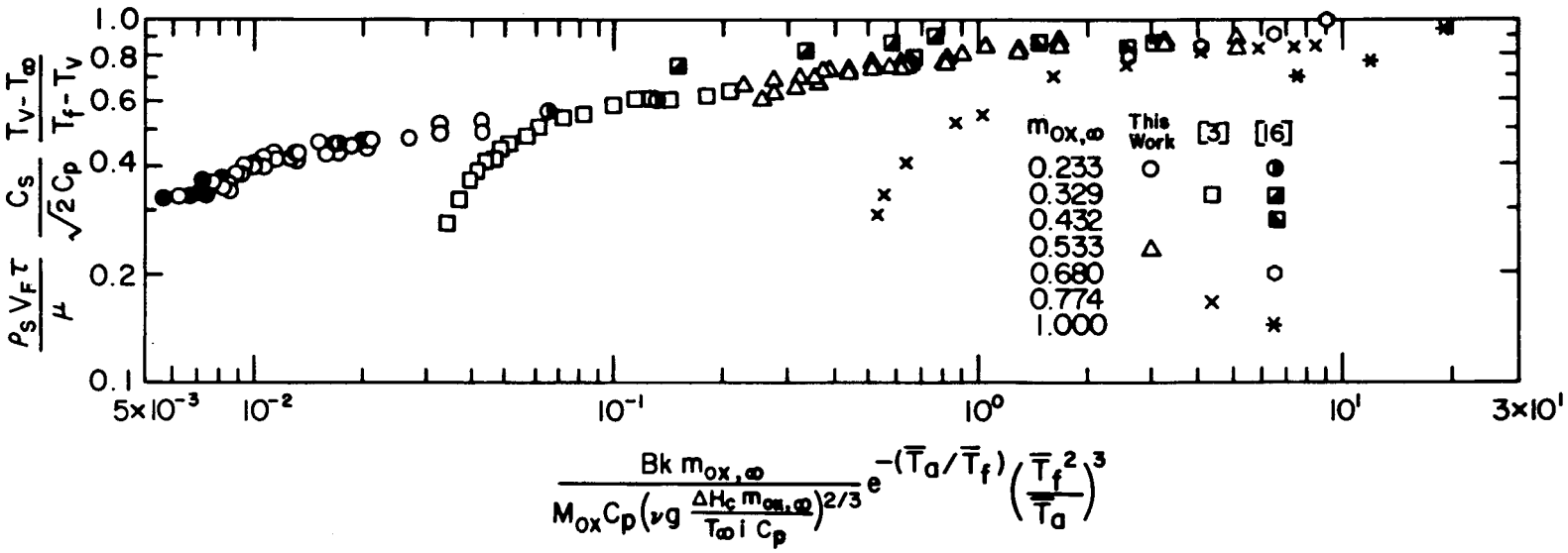

Figure 2 Dimensionless downward flame spread correlation for thin fuels [3]

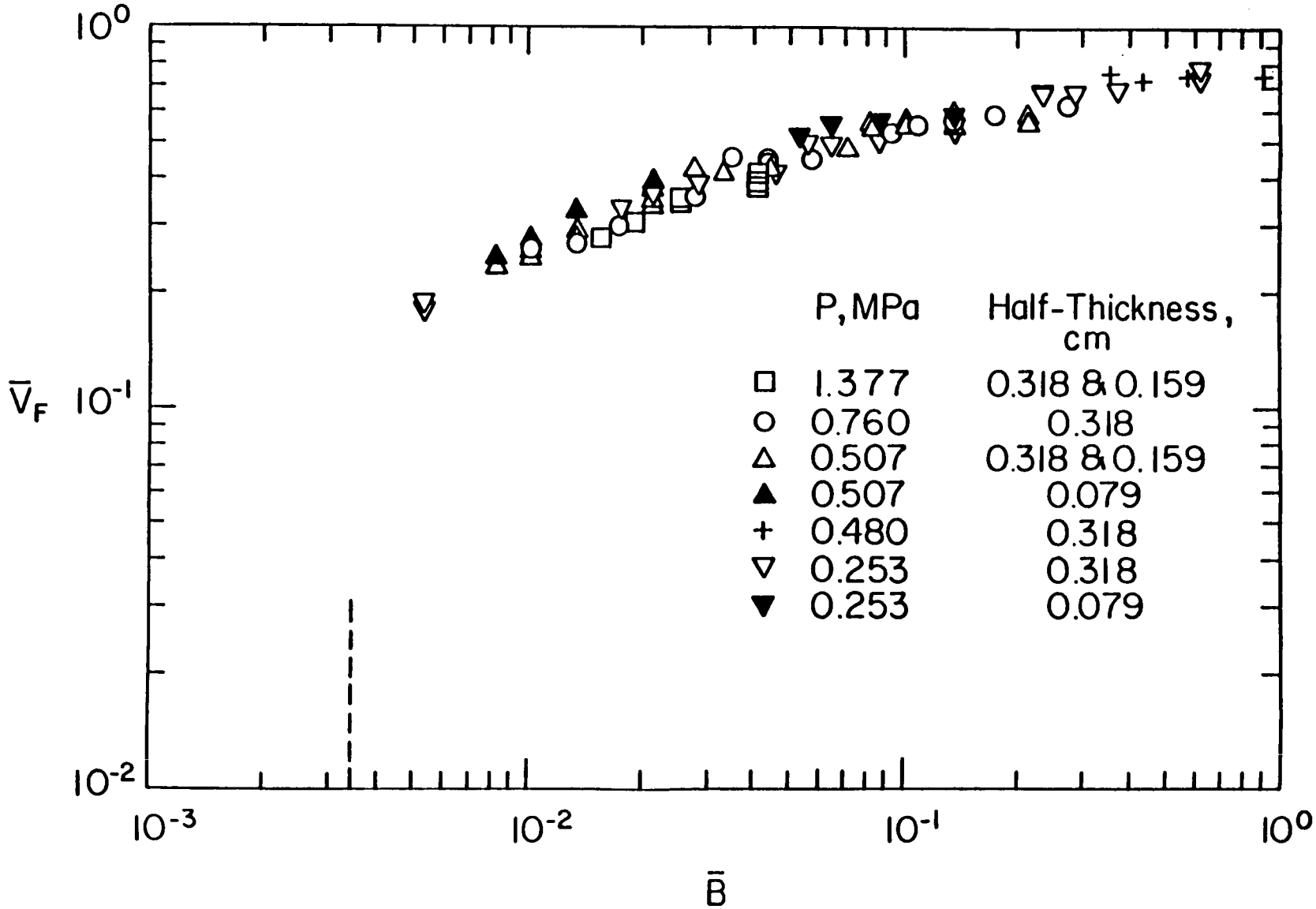

Figure 3 Dimensionless downward flame spread correlation for thick fuels [4]

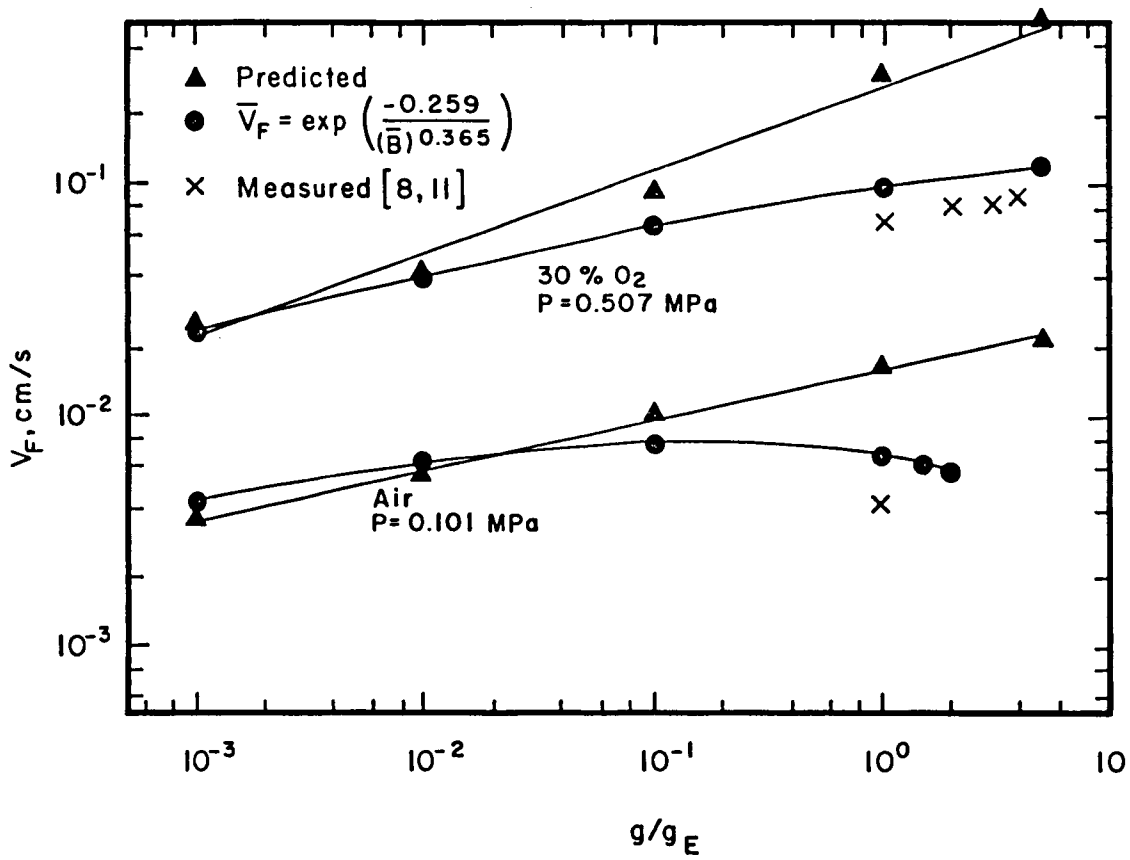

Figure 4 Predicted and Experimental Spread Rates for Spread Down a Semi-infinitely Thick, PMMA Fuel Bed as a Function of Gravitational Acceleration [17]

SOLID SURFACE COMBUSTION EXPERIMENT

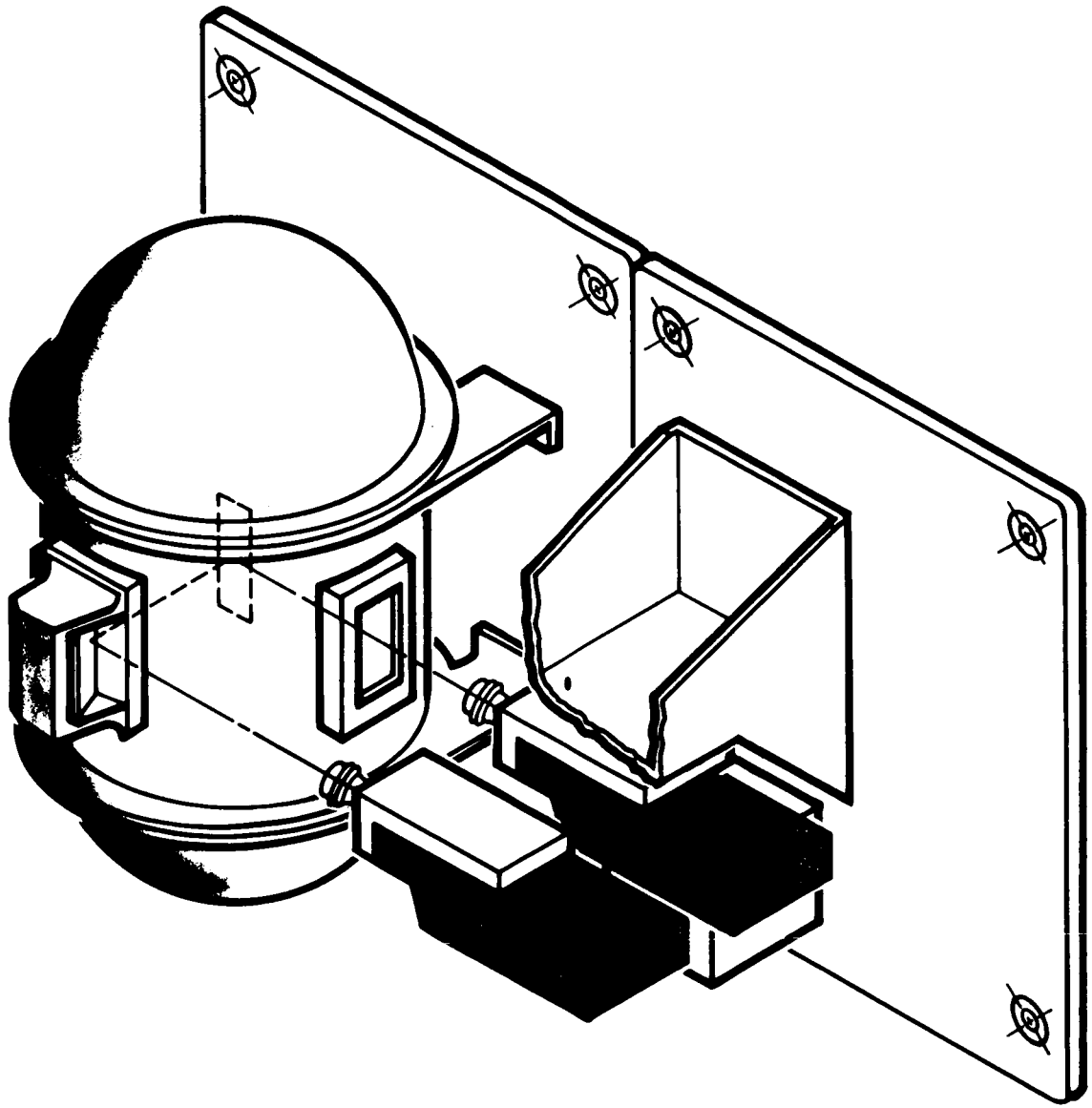

CD-84-14426

ORIGINAL PAGE IS
OF POOR QUALITY

Case 1
50% O_2
0.152 MPa

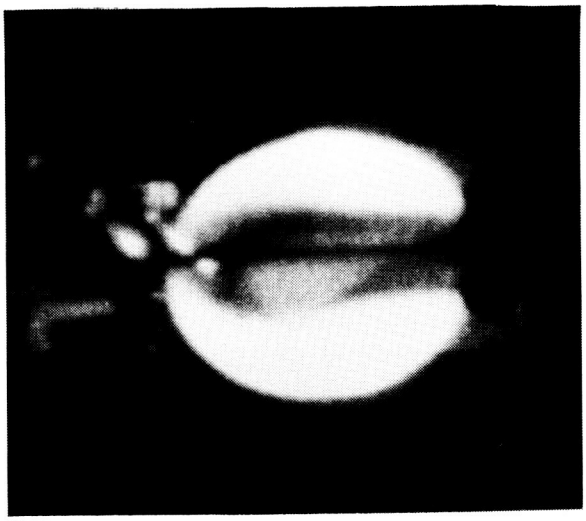

Case 2
30% O_2
0.152 MPa

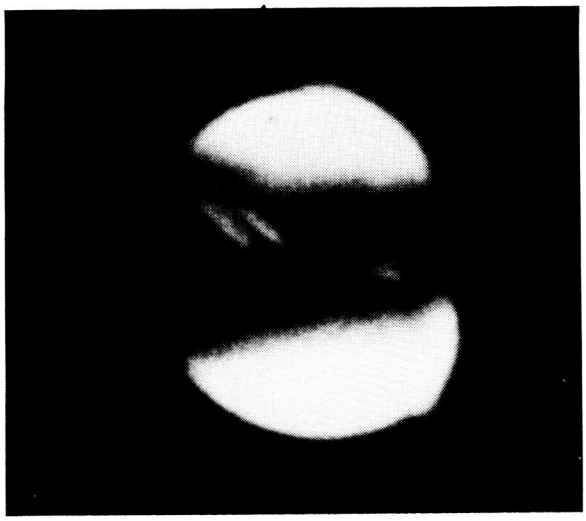

Case 3
30% O_2
0.203 MPa

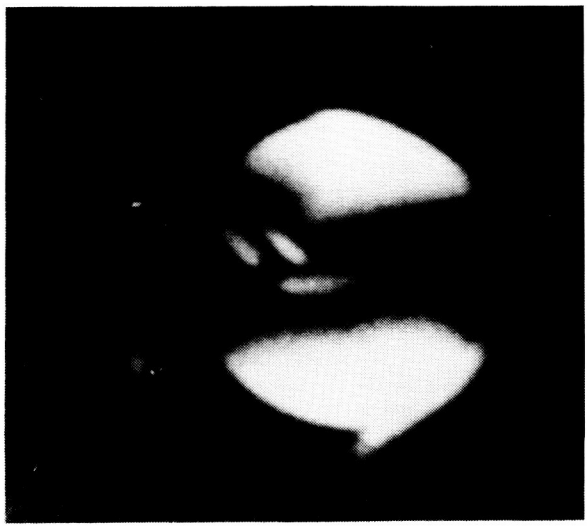

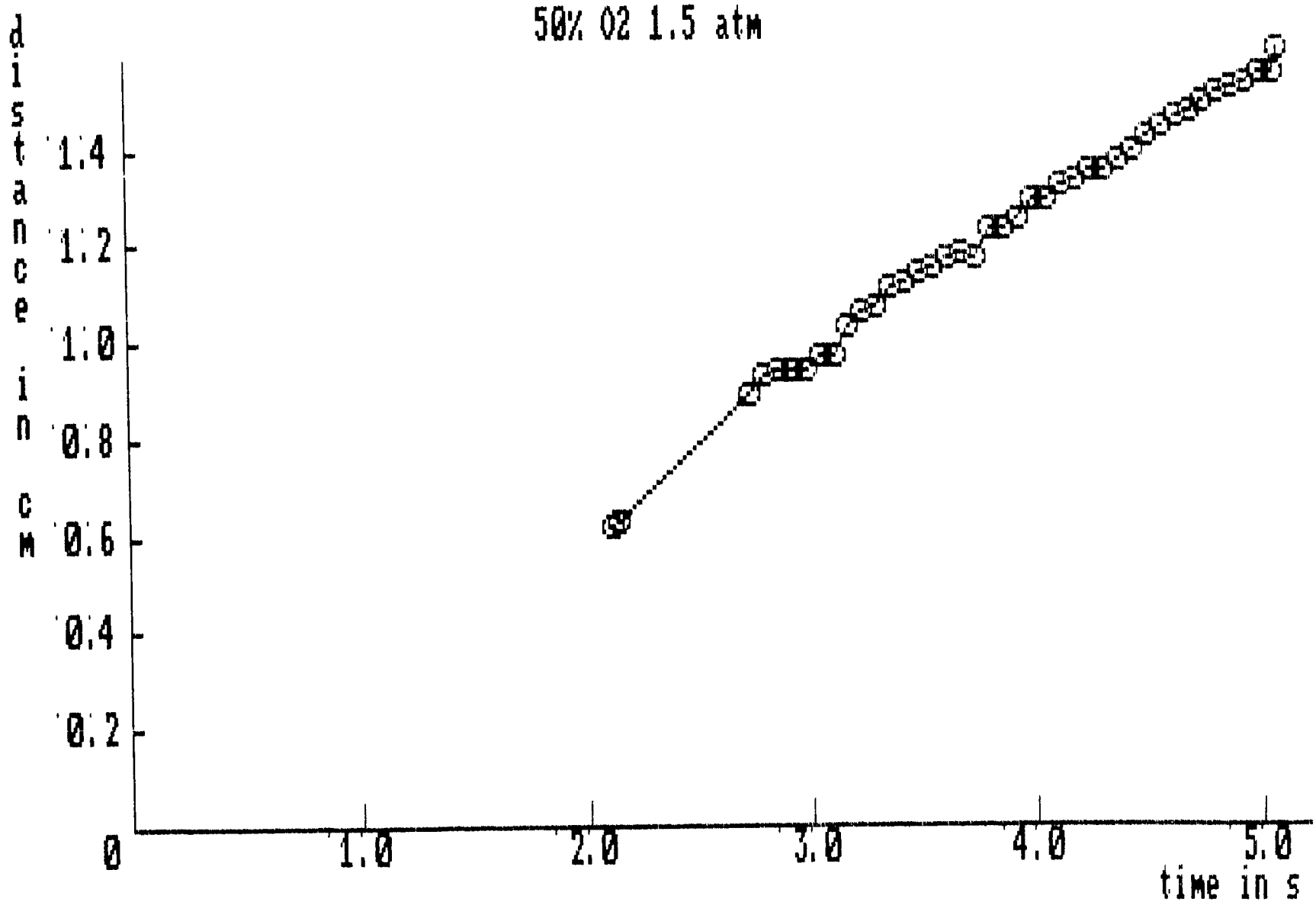

Figure 7 Position vs time for flame spreading in the 5 s droptower.

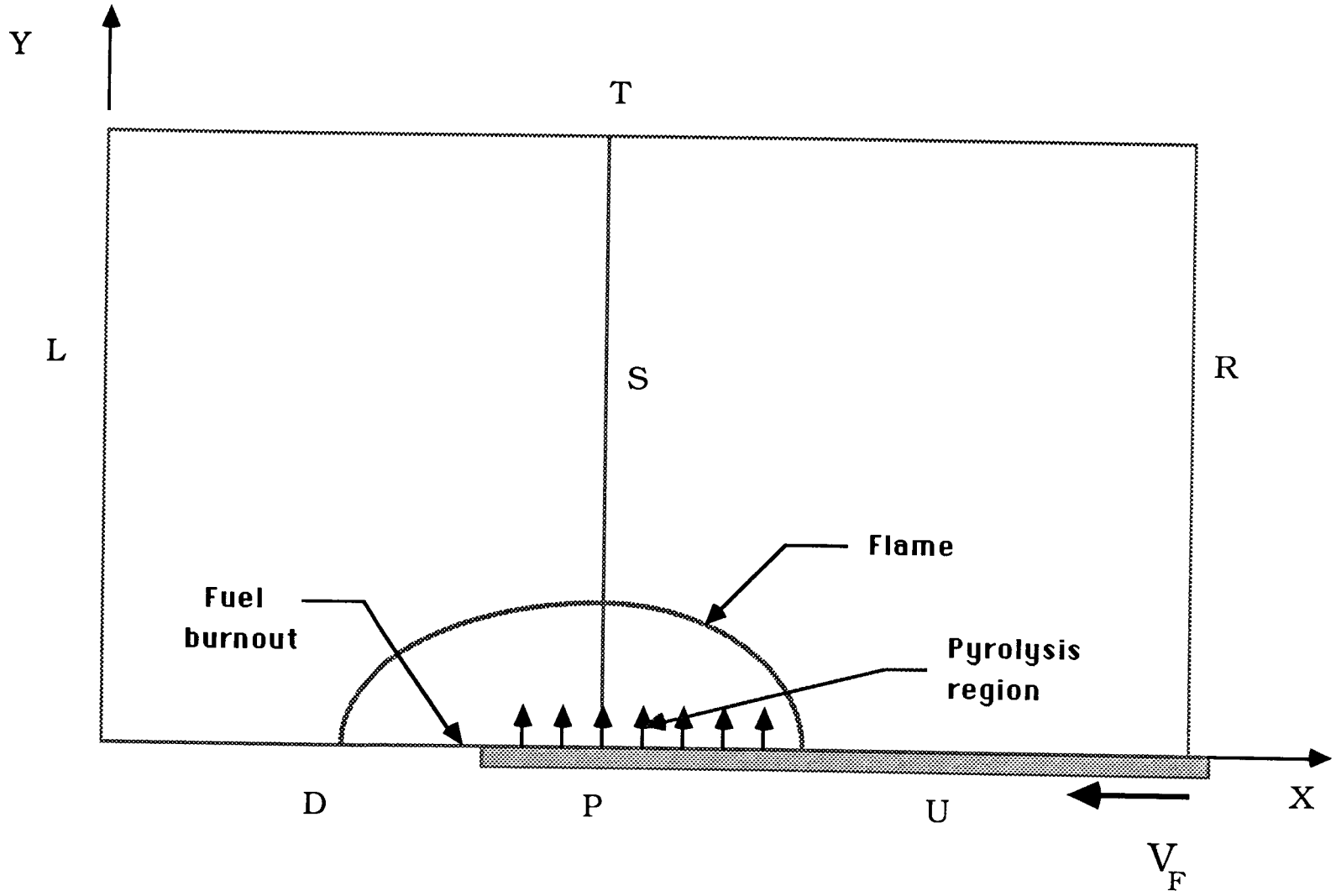

Figure 8 Computational domain.

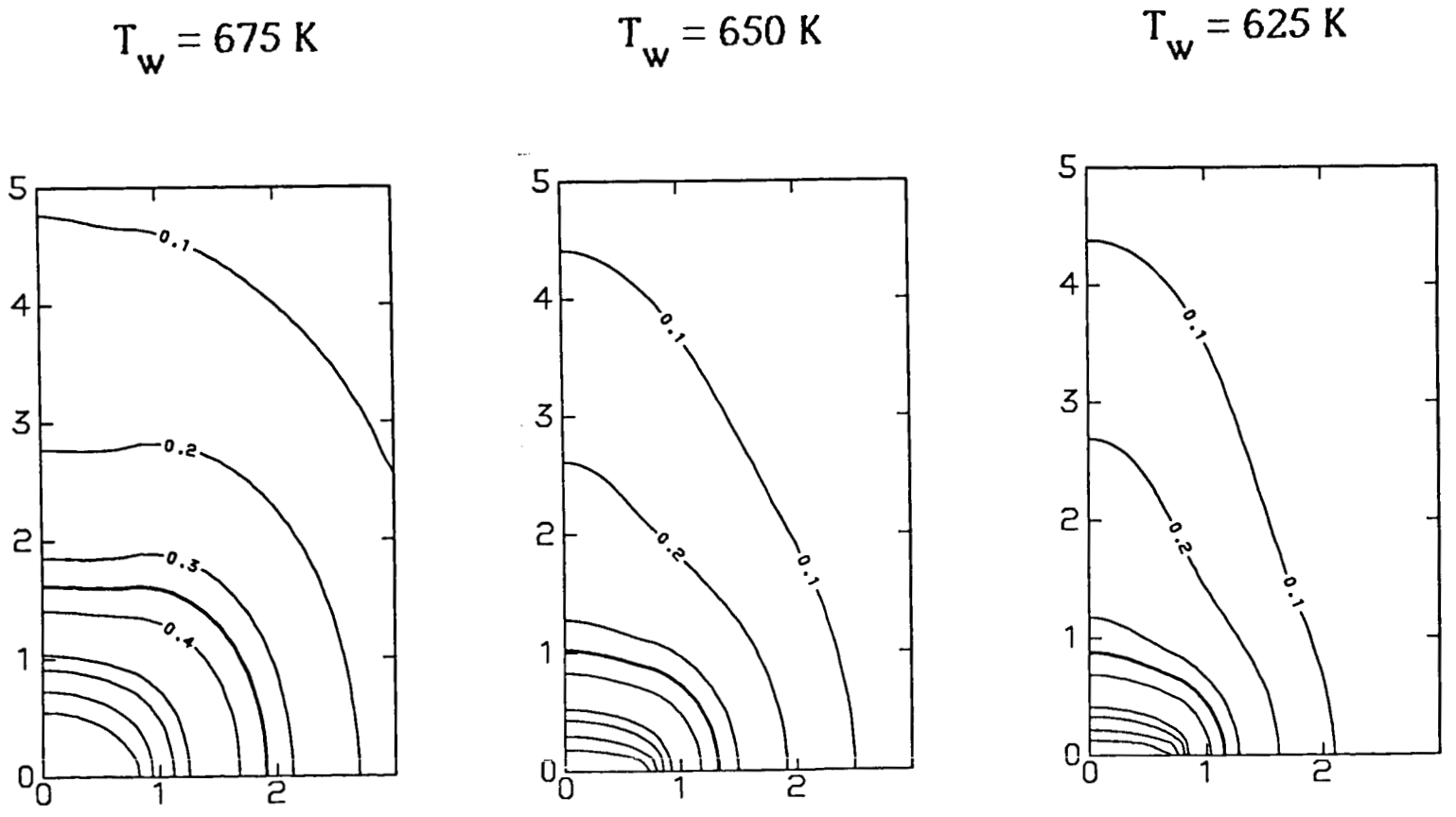

Figure 9 Coupling Function Contours for 50% O_2 , 1.5 atm (Case 1).

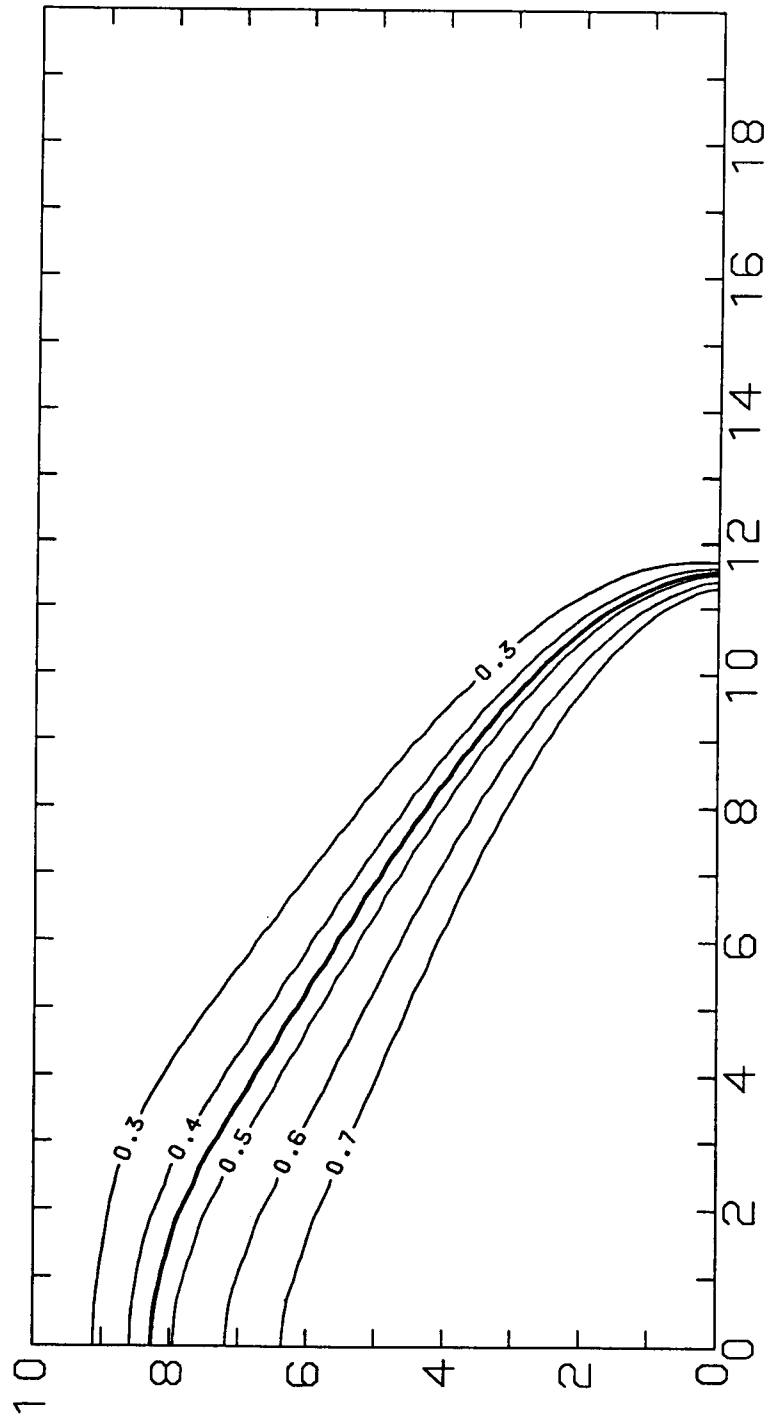

Figure 10 Coupling function field for Case 1 of Fig. 6. The length scale is α/v_r.

Figure 11 Velocity vector field for Case 1 of Fig. 6. The length scale α/v_r.

ORIGINAL PAGE IS
OF POOR QUALITY